Biomechanism and Bioenergy Research 1(1), 1-11

Thermal Performance of a Parabolic Trough Solar Concentrator Coupled with a Modified Flat Plate Collector for Greenhouse Heating

Abolfazl Ziaadini[1], Azam Noroozi[2*], Seyyed Mohammad Javadi Moghaddam[3]

[1] *Department of Biosystems Engineering, Faculty of Agriculture Shahrekord University, Shahrekord, Iran*
[2] *Department of Engineering, University of Torbat Heydarieh, Torbat Heydarieh, Iran*
[3] *Department of Computer Engineering, Bozorgmehr university of Qaenat, Qaen, Iran*

INFO

RESEARCH PAPER

KEYWORDS

Pyrolysis; Experimental validation; flow rate; greenhouse; thermal modeling

Received: *03 February 2022*

Revised: *22 March 2022*

Accepted: *24 March 2022*

Available Online: *30 March 2022*

ABSTRACT

In the present study a parabolic trough solar collector (PTC) was coupled with a modified flat plate solar collector (FPC) to serve as a greenhouse heating system. The modified FPC was located inside the greenhouse for two purposes: working as the heat exchanger during the night and also generating solar thermal energy during the day. Heat transfer models were established to describe the performance of the system components and a set of experiments were conducted to validate the models. The results showed that there was a fair agreement between the theoretical and experimental data with respect to the correlation coefficient and the root mean square percent deviation criteria. The average thermal efficiency of the PTC decreased when the FPC was engaged. Raising the fluid flow rate through the PTC increased the amount of stored energy at the off-FPC mode while it led to a decrease in stored energy when the system was at on-FPC mode.

INTRODUCTION

Greenhouse cultivation has been increased in response to population growth, reduction in available supplies and arable lands and raising the standards of living (Banaeian *et al.*, 2011).Since the quality and quantity of the products are profoundly affected by the greenhouse temperature (Vadiee and Martin, 2013); providing an appropriate heating system is an elementary must for greenhouse cultivation. The largest fraction of the energy needed for greenhouse crop production usually belongs to the heating systems (Banaeian *et al.*, 2011; PAKSOY *et al.*, 2010). Many factors such as glazing material, weather condition, water quality and product type have to be considered to design an appropriate heating system (Santamouris *et al.*, 1994; Tiwari and Dhiman, 1986). Fabrizio showed that using polycarbonate sheets as the greenhouse cover can reduce energy consumption by 20 percent compared to polyethylene sheets (Fabrizio, 2012).Yano et al. applied a semi-transparent cover made from spherical photovoltaic micro cells to minimize greenhouse energy consumption. The study concluded that the proposed system was potentially suitable for regions with high solar radiation and low winter thermal demand (Yano *et al.*, 2014). A greenhouse with a roof made from three layers of polyethylene was tested by Ureña-Sánchezin Spain (Ureña-Sánchez *et al.*, 2012).

Due to the high cost and the environmental concerns associated with the fossil fuels, renewable energy-powered heating systems such as geothermal, solar and biomass- are increasingly considered as the alternative or supplementary to the traditional fossil fuel heating equipment in greenhouses (Chau *et al.*, 2009; Ghosal and Tiwari, 2004; Hepbasli, 2005). The results of a study showed the successfully use of various renewable energy sources, including: biogas, solar and geothermal for greenhouse heating in Turkey (Esen and Yuksel, 2013). Bibbiani et al., reported that thermal load of greenhouses in Italy is ranged between 30 and 175Wm^{-2}.

They also have conducted a techno-economic analysis of wood-fuel water heating system for greenhouses. They concluded that the specific cost was between 0.032 and 0.06€.kWh^{-1} for the small boiler systems (Bibbiani *et al.*, 2016).

A number of studies have analytically or/and experimentally investigated various solar-powered systems in greenhouse air heating. Ozgener and Hepbasli developed a solar-assisted ground-source heat pump system for greenhouse heating in Izmir, Turkey. The coefficient of performance of the designed heat pump was around 2.13 and 2.84 on cloudy and sunny days, respectively (Ozgener and Hepbasli, 2005). Attar and Farhat have developed a thermal model to investigate the potential of using solar water systems for greenhouse heating in Tunisia. They reported that the proposed system could reduce the heating cost of a 1000m^3 greenhouse by 81.5% in April (Attar and Farhat, 2015). Zhou et al. developed solar energy storage and heating systems for a plastic greenhouse. They also established and experimentally verified a one-dimensional dynamic model to design and evaluate the system performance (Zhou *et al.*, 2017). Mehrpooya et al., have tried to optimize the performance of combined solar collector-geothermal heat pump systems for greenhouse heating in both economic and technical points of view. The selected model in this study presented a mean seasonal coefficient of performance of 4.14

* Corresponding Author. Email Address: azan_noroozi@yahoo.com
DOI: 10.22103/bbr.2022.18965.1004

Nomenclature

A_a	aperture area (m^2)
A_c	collector surface area (m^2)
A_r	projected area of receiver tube (m^2)
C_p	specific heat (J/kg °C)
D	diameter (m)
F'	efficiency factor of collector
F_R	heat removal factor
G	solar intensity (W/m^2)
g	acceleration of gravity (m/s^2)
H	tank height (m)
h_{fi}	convective heat transfer coefficient of working fluid (W/m^2°C)
h_r	radiation heat transfer coefficient (W/m^2 °C)
h_w	convective heat transfer coefficient of water (W/m^2 °C)
K	thermal conductivity (W/m^2 °C)
l	length of longitudinal tubes (m)
L	characteristic length of collector (m)
m	mass (kg)
$\dot{m}$	mass flow rate (kg/min)
N	number of longitudinal tubes
Nu	Nusselt number
p_c	perimeter of the collector area (m)
Q_l	thermal energy losses (W)
Q_u	useful thermal energy gain (W)
Q_{ut}	heat storage rate (W)
r_1	inner radius of tube (m)
r_2	outer radius of tube (m)
r_3	outer radius of insulator (m)
Ra	Rayleigh number
R_a	thermal resistance of greenhouse air (°C /W)
Re	Reynolds number
R_e	thermal resistance of insulator around tube (°C/W)
R_i	thermal resistance of working fluid (°C /W)
R_r	thermal resistance of tube wall (°C /W)
R_t	total thermal resistance between absorber surface and greenhouse atmosphere (°C /W)
$R_{t,tu}$	total thermal resistance between working fluid inside the tube and ambient (°C /W)
S	absorbed solar energy by receiver (W/m^2)
T	temperature (°C)
U	heat losses coefficient (W/m^2 °C)
U_l	overall heat losses coefficient (W/m^2 °C)

Greek letters

α	absorptivity of absorber tube
β	volumetric expansion coefficient (1/ °C)
γ	acceptance coefficient of receiver tube
δ	thickness of absorber plate (m)
ε	emissivity coefficient
η_o	optical efficiency (decimal)
η_{th}	thermal efficiency (%)
θ	angle of incidence of radiation on aperture (degree)
ϑ	kinematic viscosity (m^2/s)
ρ	density (kg/m^3)
σ	Stefan-Boltzmann constant (W/m^2K^4)
τ	transmittance of glass cover
ϕ	angle between solar collector and horizontal plane (degree)
ω	reflectivity of concentrator

Subscripts

a	ambient air
bot	bottom of collector
$edge$	edges of collector
f	working fluid
g	glass
gh	greenhouse
$hcoll$	horizontal collecting tubes
i	inside
ins	insulator
o	outside
p	absorber plate
ptc	parabolic trough collector
r	solar absorber tube
rec	receiver
s	surface
t	tank
top	top of collector
tu	tube
w	water

(Mehrpooya *et al.*, 2015). Hussain et al. have suggested linear and spot Fresnel lens solar concentrators for greenhouse heating in South Korea. The results of the study showed that thermal performance of spot Fresnel lens solar collector was 7-12% higher than that of linear type. They also reported that increasing the storage tank capacity enhanced thermal efficiency of the collectors (Hussain *et al.*, 2015). Anifantis et al., have experimentally investigated the performance of a combined renewable energy heating system for greenhouse heating.

The proposed system was made up of photovoltaic module that fed an electrolyzed assembly to produce hydrogen during daylight hours. During the nights, the stored hydrogen generated electricity to supply a geothermal heat pump to heat the greenhouse (Anifantis *et al.*, 2017).

The present study has proposed a novel combined solar heating system consists of a parabolic trough solar collector and a dual-purpose modified flat plate solar collector for greenhouse heating in Kerman city, Iran. The modified flat plate solar collector was located inside the greenhouse to serve as the heat exchanger during night hours. The aim of this paper is to investigate the thermal energy stored by the proposed system during daytime. Heat transfer models were established to describe the performance of the system components and a set of experiments were conducted to validate the models using statistical criteria.

MATERIALS AND METHODS

System Description

A schematic diagram of the proposed solar greenhouse heating system was indicated in fig. 1. The system was comprised of a Parabolic Trough solar Collector (PTC), a modified Flat Plate solar Collector (FPC), a heat storage tank, a pump and connecting tubes. The PTC was constructed from a shiny stainless steel sheet as the reflector, offering a good reflectivity, flexibility and stability. The absorber pipe was an evacuated tube which included a black painted cooper pipe, (diameter of 44mm and 1660mm in length) and a glass cover with outside diameter of 57.65mm. The PTC was installed in east-west orientation with tracking system in south-north direction. The FPC assembly was a sheet-and-tube solar collector possessed a black painted aluminum absorber plate (2m in length and 0.95m in width) and copper tubes (diameter of 10mm) with parallel configuration. Since the FPC was supposed to serve as a heat exchanger, to transfer heat from the storage tank to the greenhouse atmosphere during nights, besides absorption of solar irradiance during sunshine hours, its transparent cover, on the front surface was completely removed. Other sides of the FPC were insulated using glass wool materials (40mm thick).

The tank consisted of an internal heat storage container (capacity of 200L) surrounded by another cylindrical space (capacity of 25L) which acts as the heat exchanger between the circulating fluid and the inner container. Outer surface of the tank was completely insulated using 5cm thick Ethylene Propylene Diene Monomer (EPDM) materials. A centrifugal pump (UPS 15-60, Grandfos Co., Germany) was used to circulate the working fluid through the PTC assembly. The FPC assembly was designed in a manner that allows the thermal storage fluid to flow naturally through the collector. During sunshine hours, the absorber plates and therefore the fluid inside the tubes become hot. This results in density gradient and subsequently naturally movement of the fluid from the bottom to the top side of the FPC. During night hours, when the greenhouse temperature drops down, the fluid flow direction inside the FPC is reversed to transfer the stored heat from the tank to the greenhouse atmosphere via the absorber plate surface.

System Modeling

Parabolic Trough Solar Collector (PTC)

The useful thermal energy gain of the PTC ($Q_{u,ptc}$) is given by the following expression (Bergman, 2012; Kalogirou, 2013):

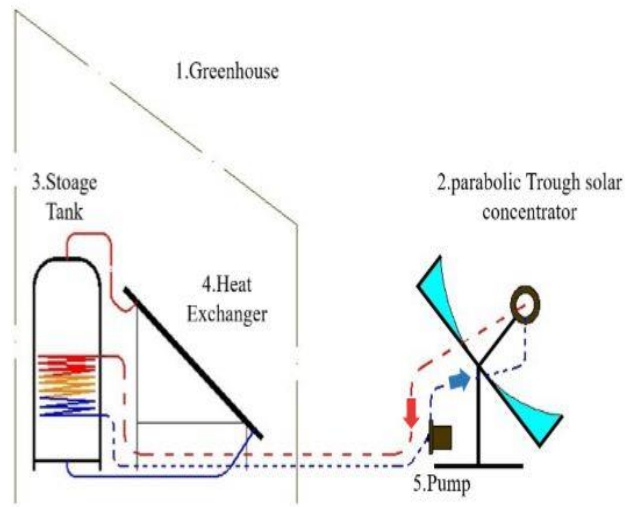

Fig. 1. Schematic diagram of the proposed solar greenhouse heating system

$$Q_{u.ptc} = F_{R.ptc}[SA_a - A_r U_{l.ptc}(T_{i.ptc} - T_a)] \quad (1)$$

where $T_{i.ptc}$ and T_a are respectively the fluid inlet and ambient temperatures, A_a and A_r are respectively the aperture area and the projected area of the receiver tube, $F_{R.ptc}$ is the heat removal factor of the receiver tube, $U_{l.ptc}$ shows the overall heat losses coefficient of the receiver and S is the absorbed solar energy by the receiver. $F_{R.ptc}$ and S are calculated by equations 2-4 (Farahat *et al.*, 2009; Kalogirou *et al.*, 2016a; Shrivastava *et al.*, 2017):

$$F_{R.ptc} = \frac{\dot{m}C_p[1-exp\left(-\frac{F'_{ptc}U_{l.ptc}A_r}{\dot{m}C_p}\right)]}{U_{l.ptc}A_r} \quad (2)$$

$$U_{l.ptc} = [\frac{A_r}{(h_{wp} + h_{r.c-a})A_a} + \frac{1}{h_{r.r-c}}]^{-1} \quad (3)$$

$$S = \eta_{o.ptc}G \quad (4)$$

where F'_{ptc} is the efficiency factor of the collector, h_{wp}, $h_{r.c-a}$ and $h_{r.r-c}$ are respectively the convective heat transfer coefficient between the receiver surface and ambient, the radiation heat transfer coefficient between the glass cover and ambient, $h_{r.r-c}$ is the radiation heat transfer coefficient between the absorber tube and glass cover, $\eta_{o.ptc}$ in equation 4 shows the optical efficiency and G is the solar radiation intensity. F'_{ptc} and η_{op} are defined as follows (Woldemichael *et al.*, 2012).

$$F'_{ptc} = \frac{1/U_{l.ptc}}{1/U_{l.ptc} + D_{o.rec}/h_{fi.rec}D_{i.rec} + (\frac{D_{o.rec}}{2K_{r.rec}} ln\frac{D_{o.rec}}{D_{i.rec}})} \quad (5)$$

$$\eta_{op} = \omega\gamma\alpha\tau[(1 - A_r\, tan(\theta))\, cos(\theta)] \quad (6)$$

where $D_{o.rec}$ and $D_{o.rec}$ are respectively the inner and outer diameters of the absorber tube, $K_{r.rec}$ is the thermal conductivity of the absorber tube, $h_{fi.rec}$ shows the convective heat transfer coefficient of the working fluid inside the receiver, α is the absorptivity of the

absorber tube, γ shows the acceptance coefficient of the receiver tube, τ stands for the transmittance of the glass cover, ω and θ are the reflectivity of the concentrator and the angle of incidence of radiation on the aperture.

The heat transfer coefficients used in equations 3 and 5 can be calculated by the following expressions (Bahrehmand *et al.*, 2015):

$$h_{wp} = \frac{(Nu_{o.rec})K_a}{D_{o.rec}} \tag{7}$$

$$h_{fi} = \frac{(Nu_{i.rec})K_w}{D_{i.rec}} \tag{8}$$

$$h_{r.c-a} = \varepsilon_g \sigma (T_{g.rec} - T_a)(T_{g.rec}^2 - T_a^2) \tag{9}$$

$$h_{r.r-c} = \frac{\sigma (T_{g.rec} - T_{r.rec})(T_{g.rec}^2 - T_{r.rec}^2)}{\frac{1}{\varepsilon_r} + \frac{A_r}{A_g}(\frac{1}{\varepsilon_g} - 1)} \tag{10}$$

where K_a and K_w are respectively the thermal conductivity of air and working fluid, ε_g and ε_r are respectively the emissivity of the glass cover and the absorber tube, $T_{g.rec}$ and $T_{r.rec}$ show the glass cover and the absorber tube surface temperatures, respectively. $Nu_{i.rec}$ in equation 6 stands for the Nusselt number which depends on the Reynolds number (*Re*) when there is a forced convective flow. The Nusselt number for laminar flow inside the circular tubes is usually considered to be 4.36 (Woldemichael *et al.*, 2012) and its value for external flow around a circular tube ($Nu_{o,rec}$) can be calculated by the following empirical expression (Bahrehmand *et al.*, 2015; Kalogirou, 2013; Woldemichael *et al.*, 2012):

$$Nu_{o.rec} = 0.3(Re)^{0.6} \tag{11}$$

The fluid outlet temperature of the PTC can be given from equation 1 as follow:

$$T_{o.ptc} = T_{i.ptc} + \frac{Q_{u.ptc}}{\dot{m}_f C_p} \tag{12}$$

where $\dot{m}_f$ and C_p are respectively the mass flow rate and the specific heat of the working fluid inside the PTC. Finally, thermal efficiency of the PTC is given by (Joudi and Farhan, 2014):

$$\eta_{th.ptc} = \frac{Q_{u.ptc}}{A_a G} \times 100 \tag{13}$$

Modified Flat Plate Solar Collector

The useful thermal energy gain of the FPC ($Q_{u.ptc}$) can be expressed as follow (Ge *et al.*, 2014; Kalogirou, 2013):

$$Q_{u.coll} = F_{R.coll} A_c [G(\tau_c \alpha_{abs}) - U_{l.coll}(T_{i.coll} - T_{gh})] \tag{14}$$

Where $T_{i.coll}$ and T_{gh} are respectively the inlet and greenhouse atmosphere temperatures, A_c shows the collector surface area, τ_c and α_{abs} are respectively the transmitivity of the greenhouse cover and the absorptivity of the flat plate absorber. The heat removal factor ($F_{R.coll}$) is calculated by (Duffie and Beckman, 2013; Kalogirou, 2013):

$$F_{R.coll} = \frac{\dot{m}_w C_p}{U_{l.coll} A_c}[1 - exp\left(-\frac{F'_{coll} U_{l.coll} A_c}{\dot{m}_w C_p}\right)] \tag{15}$$

where $\dot{m}_w$ stands for the water mass flow rate through the FPC. Since the stored water was supposed to flow naturally through the FPC tubes and storage tank, the mass flow rate can be given by the following expression (Duffie and Beckman, 2013; Khalifa and Mehdi, 1998).

$$\dot{m}_w = C^{\frac{1}{2}}[\frac{\rho_o \beta}{C_p \vartheta} F'_{coll}(G(\tau\alpha) - U_{l.coll}(T_{s.coll} - T_{i.coll})]^{\frac{1}{2}} \tag{16}$$

where $T_{s.coll}$ is the surface temperature of the absorber plate, β, ρ_o and ϑ show respectively the volumetric expansion coefficient, density and kinematic viscosity of water and C is a geometrical coefficient depends on the dimensions of the tubes. The following expression is used for determining the *C* coefficient.

$$C = \frac{gN\pi A_c D_{i.coll}^4 (\frac{l_{coll} \sin\theta}{2} + H)}{128 l_{coll}(1 + \varphi)} \tag{17}$$

where:

$$\varphi = N \frac{l_{coll}}{l_{hcoll}} (\frac{D_{i.coll}}{D_{hcoll}})^4 \tag{18}$$

In equation 18, g shows the acceleration of gravity, N, $D_{i.coll}$ and l_{coll} show respectively the number, diameter and length of the longitudinal tubes, D_{hcoll} and l_{hcoll} are respectively the diameter and the length of the two horizontal collecting tubes (at the two ends of the collector), H stands for the height of the tank and φ is an geometrical characteristics.

To calculate the value of F'_{coll} in equation 16, a useful expression is as follow (Ge *et al.*, 2014):

$$F'_{coll} = \frac{1/U_{l.coll}}{w[\frac{1}{U_{l.coll}(D_{o.coll} + (w - D_{o.coll})F)} + \frac{1}{\pi D_{i.coll} h_{fi.coll}}]} \tag{19}$$

where:

$$F = \frac{tanh\left(\sqrt{\frac{U_{l.coll}}{k_p \delta}} \frac{w - D_{o.coll}}{2}\right)}{\sqrt{\frac{U_{l.coll}}{k_p \delta}} \left(\frac{w - D_{o.coll}}{2}\right)} \tag{20}$$

where w is the distance between two tubes, $D_{o.coll}$ and $D_{i.coll}$ are respectively the outer and inner diameters of the tubes, $h_{fi.coll}$ is the convective heat transfer coefficient of the working fluid. F is the so-called standard fin efficiency factor, δ and $k_p$show respectively the thickness and the thermal conductivity of the absorber plate. To calculate the convective heat transfer coefficient of the fluid inside the collector ($h_{fi.coll}$), the following expression is used (Bahrehmand *et al.*, 2015).

$$h_{fi.coll} = \frac{(Nu_{i.coll})K_w}{D_{i.coll}} \tag{21}$$

Since there is a natural convective flow inside the FPC assembly, the Nusselt number can be calculated based on the Rayleigh number (Ra) as follow (Bergman, 2012):

$$\mathrm{Ra} = \frac{g\cos(\psi)\beta(T_{s.coll} - T_{gh})L^3}{\vartheta\alpha} \quad (22)$$

where ψ is the angle between the solar collector and the horizontal plane and L is the characteristic length of the collector which can be expressed based on the area(A_c) and the perimeter (p_c) of the collector area.

$$\mathrm{L} = \frac{A_c}{p_c} \quad (23)$$

Heat losses of the FPC included the losses from the top. the bottom and the side walls of the collector. The overall heat losses coefficient ($U_{l.coll}$) is given by (Duffie and Beckman, 2013):

$$U_{l.coll} = \mathrm{U_{top}} + \mathrm{U_{bot}} + \mathrm{U}_{edge} \quad (24)$$

where $\mathrm{U_{top}}$, $\mathrm{U_{bot}}$ and U_{edge} are respectively the heat losses coefficients of the top, the bottom and the edges of the collector. $\mathrm{U_{bot}}$ is rarely more than one tenth of the $\mathrm{U_{top}}$ value and usually is taken to be between 0.3 and 0.6 W/m^2 ^{o}C while the amount of U_e is usually between 15 and 2 W/m^2 ^{o}C (Kalogirou, 2013). $\mathrm{U_{top}}$ is given by (Duffie and Beckman, 2013; Kalogirou *et al.*, 2016b):

$$\mathrm{U_{top}} = \frac{1}{R_t A_c} \quad (25)$$

where R_t is the thermal resistance between the absorber surface and the greenhouse atmosphere and can be expressed as follow:

$$R_t = \frac{1}{A_c(h_c + h_{r.c-a})} \quad (26)$$

where $h_{r.c-a}$ and h_c are respectively the radiation heat transfer coefficient between the absorber and the surroundings and the convective heat transfer coefficient between the absorber surface and the greenhouse air. The following equation can be used for calculation of the $h_{r.c-a}$ coefficient (Duffie and Beckman, 2013):

$$h_{r.c-a} = \varepsilon_p \sigma (T_{s.coll} + T_{gh})(T_{s.coll}^2 + T_{gh}^2) \quad (27)$$

where ε_p and σ are the emissivity of the absorber plate and the Stefan-Boltzmann constant, respectively. The convective heat transfer coefficient between the absorber surface and the greenhouse air (h_c) is given by (Ghodsinezhad *et al.*, 2016):

$$h_c = \frac{(Nu_a)k_a}{L} \quad (28)$$

The Nusselt number of the air flow over the collector surface (Nu_a) can be calculated by the following empirical equation (Bergman, 2012).

$$Nu_a = 0.15 {Ra_a}^{1/3} \quad (29)$$

where Ra_a is the Rayleigh number of the natural flow of the air over the collector surface. Finally, thermal efficiency of the FPC ($\eta_{th.coll}$) is given as follow (Duffie and Beckman, 2013; Shrivastava *et al.*, 2017):

$$\eta_{th.coll} = \frac{Q_{u.coll}}{A_c G} \times 100 \quad (30)$$

Thermal Energy Storage Tank

The average rate of the thermal energy stored in the tank can be expressed as the following equation (Bergman, 2012).

$$Q_{ut} = \frac{mC_p \Delta T}{\Delta t} \quad (31)$$

where m is the water mass in the tank, ΔT is the temperature variation of the tank over the time of Δt. Since the stored energy is generated by the PTC and FTC assemblies, the energy balance equation can be written as:

$$Q_{ut} = Q_{u.ptc} + Q_{u.coll} - Q_{l.tu} - Q_{l.t} \quad (32)$$

where $Q_{l.tu}$ and $Q_{l.t}$ are the energy losses from the connecting tubes and the tank, respectively. $Q_{l.tu}$ is given by (Bergman, 2012; Kalogirou, 2013):

$$Q_{l.tu} = \frac{T_{i.tu} - T_a}{R_{t.tu}} \quad (33)$$

where $T_{i.tu}$ is the temperature of fluid inside the tube and $\mathrm{R}_{t.tu}$ is the total thermal resistance between the working fluid inside the tube and ambient air which is calculated as:

$$\mathrm{R}_{t.tu} = R_i + R_{tu} + R_{ins} + R_{a.tu} \quad (34)$$

where $R_{i,tu}$, R_{tu}, R_{ins} and $R_{a,tu}$ are respectively the thermal resistances of the working fluid, the tube wall, the insulator around the tube and the air which can be given as follows:

$$R_{i.tu} = \frac{1}{h_{i.tu} l_{tu} 2\pi r_1} \quad (35)$$

$$R_{tu} = \frac{\ln({}^{r_2}/_{r_1})}{2\pi k_r l_{tu}} \quad (36)$$

$$R_{ins} = \frac{ln({}^{r_3}/_{r_2})}{2\pi k_e l_{tu}} \quad (37)$$

$$R_{a.tu} = \frac{1}{h_{a.tu} l_{tu} 2\pi r_3} \quad (38)$$

where *l* is the tube length, $h_{i.tu}$ shows the convective heat transfer coefficient of the working fluid which can be obtained by equation 8, $r_1.r_2$ and r_3 are respectively the inner and outer radiuses of the connecting tube and the outer radius of the insulator, k_r and k_p stand for the conductivity of the tube and the insulator $h_{a.tu}$ shows the convective heat transfer coefficient of the air around the tube which was given by equation 7.

Experimental Procedure

The experiments were carried out in Biosystems engineering campus of Shahid Bahonar University of Kerman, Iran during January and February 2016. A greenhouse (area of 10m^2), constructed from a

steel frame and covered with 10mm-thick polycarbonate sheets, was used for evaluation of the solarheating system. The FPC and the thermal storage tank were installed inside and the PTC assembly was located beside the greenhouse. A photograph of the designed solar heating system and the greenhouse is illustrated in fig. 2. The tests were conducted at three different fluid flow rates through the PTC (0.5, 0.75 and 1.5kg/min) and two operating modes of the heating system including with and without FPC, named "on-FPC" and "off-FPC" modes, respectively. Each test continued during sunshine hours of the day. To inactivate the FPC, its front surface was completely covered with an opaque sheet and a shut off valve was used to stop the water flow from the tank to the FPC. A number of temperature sensors (SMT 160) were used to measure temperature of thermal storage tank at five different depths (0, 15, 30, 45 and 60 cm) as well as ambient, greenhouse, PTC inlet and outlet temperatures. The temperature sensors were connected to a personal computer by means of a temperature transmitter interface (TM-1323, Tika Eng. Co., Iran). Solar intensity on the PTC and FPC surfaces was measured using a pyrometer (TES 1333, TES Co., Taiwan). To measure wind speed during the test period a digital anemometer (BE816A, Bestone Co., China) was used.

Fig. 2. A photograph of the designed solar heating system and the greenhouse; a) The modified FPC and the tank inside the greenhouse and b) the PTC assembly

Experimental verification of the analytical models was conducted using regression coefficient (r) and root mean square percent deviation (e) criteria which were determined as follows (Mortezapour *et al.*, 2012)

$$r = \frac{n\sum X_i Y_i - (\sum X_i)(\sum Y_i)}{\sqrt{n\sum X_i^2 - (\sum X_i)^2}\sqrt{n\sum Y_i^2 - (\sum Y_i)^2}} \quad (39)$$

$$e = \sqrt{\frac{\sum (e_i)^2}{n}} \quad (40)$$

$$e_i = \frac{X_i - Y_i}{X_i} \quad (41)$$

where X_i and Y_i are respectively the ith analytical and experimental data and n shows the number of observations.

RESULTS AND DISCUSSION

Variations of solar radiation intensity, ambient temperature, wind speed, inlet and outlet fluid temperatures of the PTC at the flow rate of 0.5 kg/min and the on-FPC mode of operation on February 6, 2016 are illustrated in table 1. The statistical comparison results of the analytical and experimental outlet temperatures are also given in table 1. The observation showed that ambient temperature varied between 13.72 and 26.92 and the maximum temperature occurred at 12:30 p.m... Wind speed was low at the morning hours but its value reached to about 5 m/s at 15 p.m.. The highest solar intensity on the reflector surface was about 1098W/m^2 at 12 noon. The PTC outlet temperature had an increasing trend until 15 p.m. under the influence of the tank temperature. The maximum PTC outlet temperature was 62°C at 12 noon. Deviation between the analytical and experimental data was lower than 2.9^{o}C and it can be said according to the comparison criteria that the obtained models can fairly predict the experiment results.

Variations of ambient conditions and comparison of the calculated and the measured PTC outlet temperature at flow rate of 0.5kg/min without engaging the FPC were indicated in table 2. The given results are based on the observations made on February 7, 2016. The minimum and the maximum ambient temperatures during the time of test were 12.39 and 28.16^{o}C, respectively. The highest wind speed was about 5m/s at 15 p.m. It was also observed that the variation range of the PTC inlet temperature was between 26.32 and 33.79^{o}C lower than that of with the FPC. This means that the tank temperature is higher when the FPC is engaged. Investigation of the comparison criteria showed that the average deviation between analytical and experimental data was about 1.5^{o}C. It can also be concluded that the calculations have accurately predicted the PTC outlet temperature with respect to regression coefficient and root mean square percent deviation values. Comparing tables 1 and 2 clearly shows that the accuracy of the analytical expressions was lower at the mode of on-FPC mainly due to the errors associated with the FPC assembly equations

Thermal efficiency of the PTC at the different flow rates and modes of operation was depicted in fig. 3. It is clear that thermal efficiency decreased with engaging the FPC and it can be said that the average efficiency of the PTC without FPC was approximately 1% more than that with FPC. This arises from the fact that the tank temperature and subsequently the PTC inlet temperature are higher if the FPC is connected at the same surrounding and operation conditions. On the other hand, increasing the inlet temperature of solar collectors decreases useful thermal energy gain by the working fluid which results in thermal efficiency drop of the collectors (Bergman, 2012; Kalogirou, 2013). This finding is in accordance with the results of a study that showed that increasing the storage tank capacity improved thermal efficiency of the collectors (Hussain *et al.*, 2015).

Table 1. Variations of ambient conditions and comparison of analytical and experimental PTC outlet temperatures at the flow rate of 0.5kg/min and the on-FPC mode of operation during the day

Time	Ambient Temperature (ºC)	Wind Speed (ms^{-1})	Solar Irradiance (Wm^{-2})	Inlet Temperature (ºC)	Analytical Outlet Temperature (ºC)	Experimental Outlet Temperature (ºC)	Comparison Criteria		
							Deviation (ºC)	r	e
07:30	13.72	2.50	249.00	27.34	31.99	32.31	0.32		
08:00	17.61	2.50	393.00	28.14	35.88	35.17`	-0.71		
08:30	18.58	3.00	575.25	30.25	41.69	43.27	1.58		
09:00	20.10	3.50	677.25	31.15	44.69	47.16	2.47		
09:30	20.66	4.00	740.00	31.78	46.60	49.04	2.44		
10:00	22.12	4.00	800.00	32.47	48.53	51.33	2.80		
10:30	22.38	4.00	883.50	32.67	50.44	52.41	1.97		
11:00	24.26	4.00	971.25	33.12	52.71	54.24	1.53		
11:30	24.66	4.00	1086.75	33.69	55.63	58.53	2.90	0.96	0.041
12:00	26.39	4.00	1098.00	35.52	57.62	60.41	2.79		
12:30	26.92	4.00	1085.25	36.02	57.85	60.72	2.87		
13:00	26.60	4.20	1052.00	36.8٠	57.90	60.15	2.25		
13:30	26.22	4.35	1015.50	37.43	57.74	59.46	1.72		
14:00	25.74	4.50	891.75	38.32	56.05	56.23	0.18		
14:30	25.31	4.65	700.00	39.17	52.94	51.76	-1.18		
15:00	24.49	4.85	520.50	39.54	49.61	47.44	-2.17		
15:30	23.42	5.00	360.75	38.77	45.58	42.88	-2.70		

Table 2. Variations of ambient conditions and comparison of analytical and experimental PTC outlet temperatures at the flow rate of 0.5kg/min and the off-FPC mode of operation during the day

Time	Ambient Temperature (ºC)	Wind Speed (ms^{-1})	Solar Irradiance (Wm^{-2})	Inlet Temperature (ºC)	Analytical Outlet Temperature (ºC)	Experimental Outlet Temperature (ºC)	Comparison Criteria		
							Deviation (ºC)	r	e
07:30	12.39	3.00	222.75	26.32	30.38	30.12	-0.26		
08:00	13.42	3.25	399.75	27.41	35.18	33.87	-1.31		
08:30	16.64	3.25	542.75	28.75	39.55	40.27	0.72		
09:00	18.68	3.50	666.00	30.12	43.50	4٦.24	٢.74		
09:30	20.85	3.50	800.00	30.78	46.99	49.٨3	2.٨4		
10:00	21.19	3.70	920.00	31.01	49.71	52.26	2.55		
10:30	21.82	3.75	1010.75	31.45	52.04	53.71	1.67		
11:00	24.45	3.75	1078.25	31.89	53.96	55.12	1.16		
11:30	23.12	4.00	1116.00	31.99	54.79	57.42	2.63	0.98	0.045
12:00	25.35	4.00	1135.50	32.14	55.42	58.36	2.94		
12:30	25.8	4.25	1111.50	32.47	55.26	57.89	2.63		
13:00	28.16	4.50	1040.50	33.23	54.61	56.75	2.14		
13:30	26.4	4.50	930.00	33.79	52.79	55.39	2.60		
14:00	26.16	4.60	730.00	33.44	48.30	51.23	2.93		
14:30	26.48	4.60	514.50	32.87	43.30	44.26	0.96		
15:00	23.55	4.85	286.50	32.43	38.04	37.45	-0.59		
15:30	22.73	5.00	180.00	30.91	34.34	33.1	-1.24		

Ambient temperature is another effective factor on thermal efficiency. Total heat losses from the receiver increases at lower ambient temperatures because of the increase in temperature gradient between working fluid inside the receiver tube and its surroundings (Bergman, 2012; Dincer and Rosen, 2012; Duffie and Beckman, 2013).This may be the main reason for efficiency drop at the early and late hours of the test in each day. Fig. 3 also indicated that thermal efficiency improved with the flow rate. Increasing the

flow rate from 0.5 to 1.5 kg/min led to an average increase of 4 per cent in thermal efficiency. Refer to equation 3, increasing the flow rate leads to increase in heat removal factor which subsequently enhances useful thermal energy gain and efficiency of the PTC. Similar results were reported by (Conrado *et al.*, 2017; Yılmaz and Söylemez, 2014). Finally, the highest average thermal efficiency was found to be about 53% at the flow rate of 1.5kg/min when the FPC was inactivated.

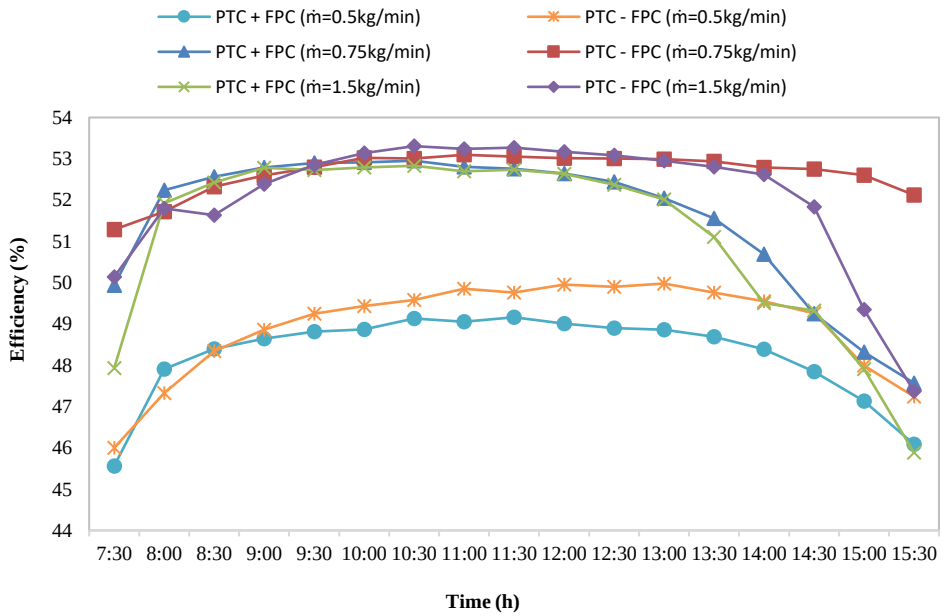

Fig. 3. Variations of the PTC efficiency at the different fluid flow rates and modes of operation

Temperatures of the greenhouse, inlet, and analytical and experimental outlet fluid of the FPC as well as average temperature of the absorber surface during February 6, 2016 were indicated in table 3. Inlet temperature had an increasing trend over the test hours and increased from 30.5ºC at 7:30 a.m. to more than 48ºC at 15:30 p.m. due to increase in tank temperature during the day. The highest average temperature of the absorber was about 66ºC which was observed around 13:00 p.m.. Furthermore, the measured outlet temperature reached to about 69ºC at the same time as the highest absorber temperature occurred. Also table 3 clearly illustrated that the fluid mass flow rate through the FPC changed with the absorber temperature (Bahrehmand *et al.*, 2015) and it soared from 4.4g/s at 7:30 a.m. to 8.8g/s at around 13:00 p.m.. It can be concluded from the regression coefficient and the root mean square percent deviation criteria that the predicted outlet temperatures of the FPC are suitably in accordance with the corresponding measured values.

Fig. 4 has depicted thermal efficiency of the FPC at the three different fluid flow rates inside the PTC. It is clear from fig. 4 that increasing the flow rate decreased thermal efficiency of the FPC. The reason perhaps is that the FPC inlet temperature is higher at the higher flow rates due to more useful thermal energy gain from the PTC. This finding is in accordance with the results of (Jafarkazemi and Ahmadifard, 2013) which indicated that increasing the inlet temperature intensified the overall heat losses from the collector. The maximum thermal efficiency was observed about 38 per cent at the flow rate of 0.5kg/min. Since increase in temperature gradient between the absorber and ambient leads to increase in thermal losses from the collector surface (Bergman, 2012; Duffie and Beckman, 2013), thermal efficiency of the FPC dropped down when surface temperature of the absorber was much more than the greenhouse temperature. The observation shows that the average efficiencies of the FPC at the flow rates of 0.5, 0.75 and 1.5kg/min were found to be about 37.5, 34.7 and 31.8 per cent, respectively

Hourly temperature rise of the thermal storage tank at the three different flow rates and two modes operation was indicated in fig. 5. With respect to the values of regression coefficient (between 0.88 and 0.98) and root mean square percent deviation (between 0.15 and 0.82) it can be said that the performed calculations could suitably predict variations of the tank temperature over the test period. Meanwhile, fig. 5-a shows that the highest hourly temperature rise while the FPC was engaged was observed to be 5.5ºC at the lowest flow rate (0.5kg/min). While, it can be seen from fig. 5-b that the highest temperature rise at the mode of off-FPC was about 3ºC at the highest flow rate (1.5kg/min). The tank temperature rise clearly soared around noon because of the suitable solar radiation and ambient temperature.

Table 3. Comparison of analytical and experimental outlet temperatures of the FPC during the day at the fluid flow rate of 0.5 kg/min

Time	Greenhouse Temperature (°C)	Absorber Temperature (°C)	Inlet Temperature (°C)	fluid mass flow (g/s)	Analytical Outlet Temperature (°C)	Experimental Outlet Temperature (°C)	Comparison Criteria		
							Deviation (°C)	r	e
07:30	25.31	36.42	30.57	4.41	37.67	37.30	-0.37		
08:00	26.98	38.10	30.79	5.50	41.74	39.94	-1.81		
08:30	28.30	42.09	31.15	6.64	45.58	42.57	-3.01		
09:00	30.98	47.14	32.42	6.83	48.66	48.07	-0.59		
09:30	33.13	50.20	33.23	7.34	50.63	53.58	2.95		
10:00	35.10	54.30	34.71	7.48	52.95	55.19	2.24		
10:30	37.17	56.44	35.31	7.85	54.93	57.80	2.87		
11:00	38.36	64.80	36.15	8.36	56.75	60.55	3.80		
11:30	41.03	61.14	37.36	8.72	59.72	63.23	3.51	0.98	0.05
12:00	42.91	62.57	39.38	8.74	61.82	64.47	2.65		
12:30	43.98	64.10	41.39	8.76	63.48	67.04	3.56		
13:00	44.94	65.66	43.37	8.59	64.83	68.12	3.29		
13:30	45.57	65.65	45.35	8.38	66.11	69.22	3.11		
14:00	45.00	64.95	47.46	7.84	66.09	68.69	2.60		
14:30	42.21	58.84	48.13	7.36	63.38	66.23	2.85		
15:00	38.63	57.00	48.30	6.25	59.40	63.32	3.09		
15:30	33.19	50.60	48.80	5.48	54.00	61.74	3.04		

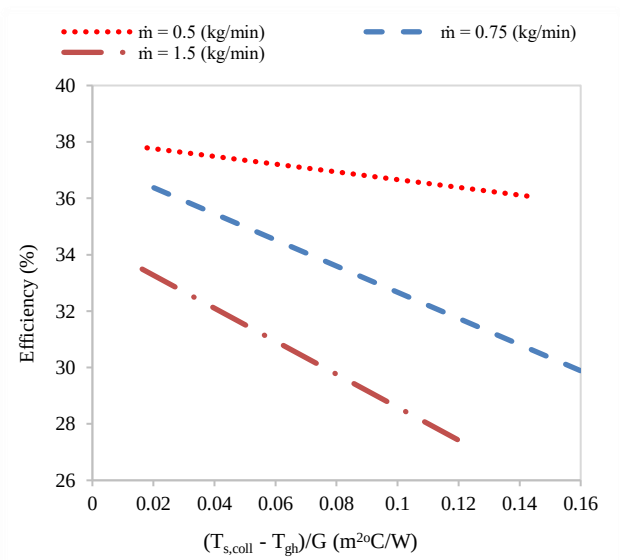

Fig. 4. Variations of thermal efficiency of the FPC during the day

Fig. 6 showed variations of stored energy at the three different flow rates and two modes of operation. It is clear from fig. 6 that high slopes of the curves were observed over 10 a.m. to 13 p.m. because of the suitable thermal energy generation of the heating system due to suitable solar radiation and ambient temperature. After that, stored energy plateaued due to reduction in solar intensity and perhaps increase in tank temperature which declines energy gain from the working fluids. As it was expected, amount of stored energy enhanced when the FPC was engaged and it can be said that stored energy at the mode of on-FPC was averagely three times more than that of off-FPC mode.

Fig. 6 also indicates that raising the flow rate at the mode of off-FPC led to an increase in the amount of stored energy. The main reason is that at this mode, thermal efficiency of the PTC, as the only thermal energy generator of the system, improved with flow rate. Vice versa, when the FPC was employed beside the PTC, increasing the flow rate decreased total thermal energy generation over the day. Raising the flow rate, on the one hand, improves thermal efficiency of the PTC, but on the other hand it drops the FPC efficiency. This finally caused a reduction in total energy generation of the solar heating system, taking into account the dimensions of the FPC and PTC

.

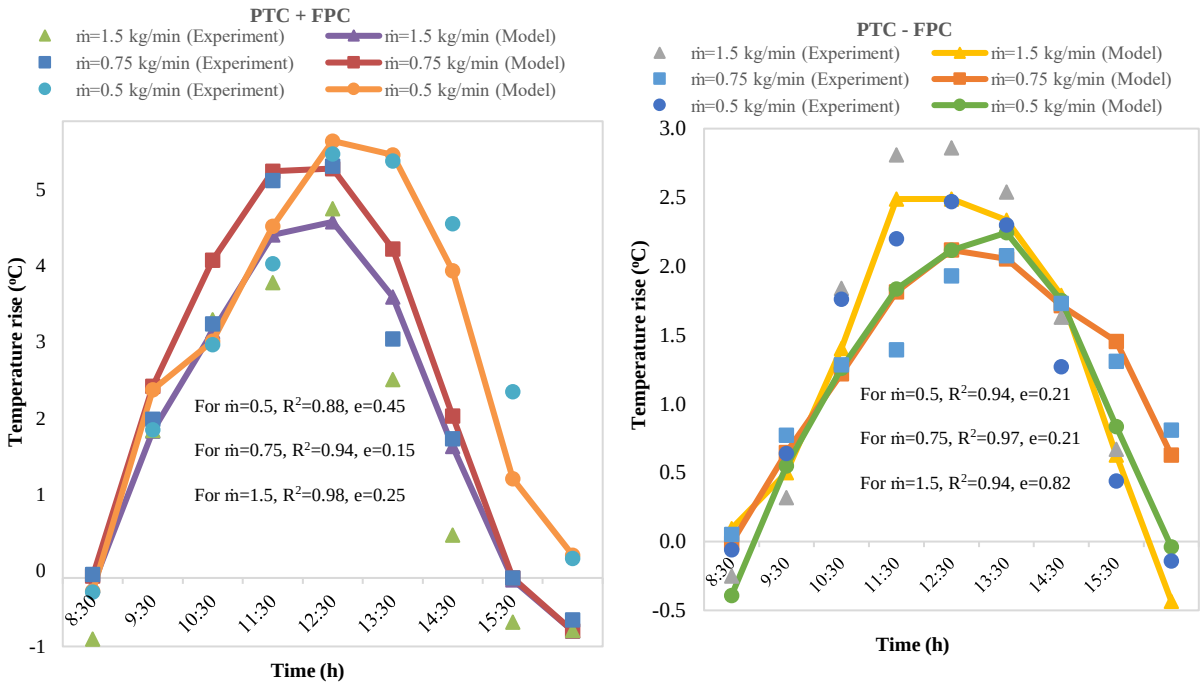

(a) (b)

Fig 5. Hourly temperature rise of the thermal storage tank at the three different flow rates and two modes of on-FPC (a) and off-FPC (b)

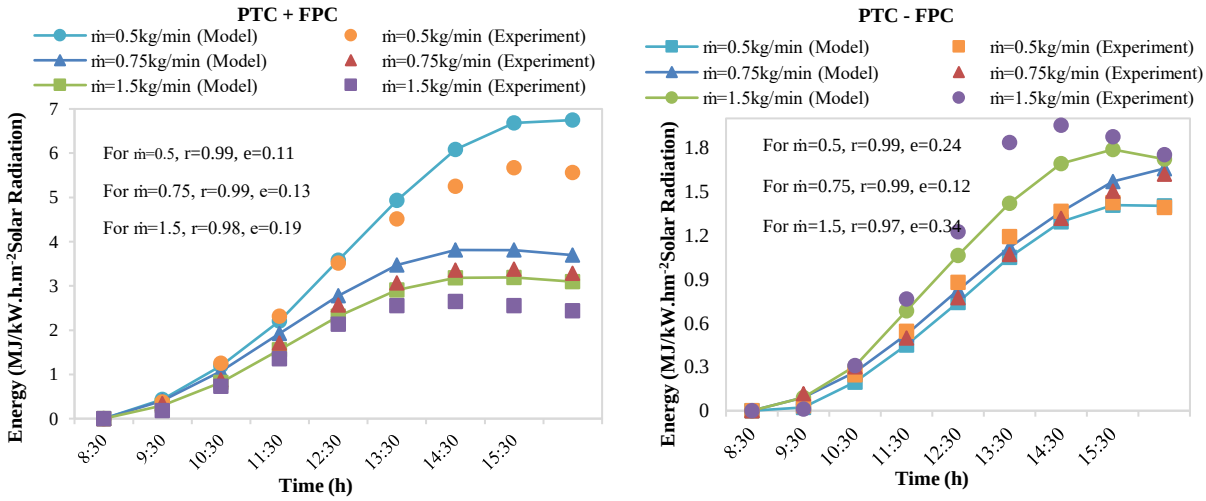

(a) (b)

Fig. 6. Variations of stored energy at the three different flow rates and two modes of on-FPC (a) and off-FPC (b)

CONCLUSIONS

The present study carried out the thermal assessment of a solar heating system consists of a parabolic trough solar collector and a dual-purpose modified flat plate solar collector for greenhouse heating. The tests were conducted at three different fluid flow rates through the PTC and two operating modes of the heating system. Experimental verification of the analytical models was conducted using regression coefficient and root mean square percent deviation criteria. The results revealed that:

- There was a suitable agreement between the obtained analytical expressions and the experimental data based on root mean square percent deviation and regression coefficient criteria.
- Increasing of the fluid flow rate through the PTC decreased thermal efficiency of the FPC and the highest thermal efficiency was observed about 38.8% at the flow rate of 0.5kg/min.

- Average efficiency of the PTC slightly decreased when the FPC was engaged.
- Stored energy was significantly higher at the mode of on-FPC compared with off-FPC mode.
- Increasing the flow rate at the mode of off-FPC improved stored energy while, it resulted in a decline in stored energy when the FPC was employed beside the PTC.
- Finally, it was concluded based on the amounts of stored energy that coupling the modified FPC with the existing greenhouse heating systems could be suggested as a simple-structure approach for improving thermal performance of the system. In this way, the performance analysis of the FPC during the nights, when it works as a heat exchanger to transfer the stored heat to the greenhouse atmosphere, can be considered in the future studies

REFERENCES

Anifantis, AS, Colantoni, A and Pascuzzi, S (2017). Thermal energy assessment of a small scale photovoltaic, hydrogen and geothermal stand-alone system for greenhouse heating. *Renewable Energy,* 103**,** 115-127.

Attar, I and Farhat, A (2015). Efficiency evaluation of a solar water heating system applied to the greenhouse climate. *Solar Energy,* 119**,** 212-224.

Bahrehmand, D, Ameri, M and Gholampour, M (2015). Energy and exergy analysis of different solar air collector systems with forced convection. *Renewable Energy,* 83**,** 1119-1130.

Banaeian, N, Omid, M and Ahmadi, H (2011). Energy and economic analysis of greenhouse strawberry production in Tehran province of Iran. *Energy Conversion and Management,* 52**,** 1020-1025.

Bergman, TL 2012. Adrienne S. lavine, Frank P. Incropera, David, Introduction to Heat Transfer. John Wiley & Sons. Inc.

Bibbiani, C, Fantozzi, F, Gargari, C, Campiotti, CA, Schettini, E and Vox, G (2016). Wood Biomass as Sustainable Energy for Greenhouses Heating in Italy. *Agriculture and Agricultural Science Procedia,* 8**,** 637-645.

Chau, J, Sowlati, T, Sokhansanj, S, Preto, F, Melin, S and Bi, X (2009). Economic sensitivity of wood biomass utilization for greenhouse heating application. *Applied Energy,* 86**,** 616-621.

Conrado, LS, Rodriguez-Pulido, A and Calderón, G (2017). Thermal performance of parabolic trough solar collectors. *Renewable and Sustainable Energy Reviews,* 67**,** 1345-1359.

Dincer, I and Rosen, MA (2012). *Exergy: energy, environment and sustainable development,* Elsevier Ltd.

Duffie, JA and Beckman, WA (2013). *Solar engineering of thermal processes,* Wiley New York.

Esen, M and Yuksel, T (2013). Experimental evaluation of using various renewable energy sources for heating a greenhouse. *Energy and Buildings,* 65**,** 340-351.

Fabrizio, E (2012). Energy reduction measures in agricultural greenhouses heating: Envelope, systems and solar energy collection. *Energy and Buildings,* 53**,** 57-63.

Farahat, S, Sarhaddi, F and Ajam, H (2009). Exergetic optimization of flat plate solar collectors. *Renewable Energy,* 34**,** 1169-1174.

Ge, Z, Wang, H, Wang, H, Zhang, S and Guan, X (2014). Exergy analysis of flat plate solar collectors. *Entropy,* 16**,** 2549-2567.

Ghodsinezhad, H, Sharifpur, M and Meyer, JP (2016). Experimental investigation on cavity flow natural convection of Al_2O_3–water nanofluids. *International Communications in Heat and Mass Transfer,* 76**,** 316-324.

Ghosal, M and Tiwari, G (2004). Mathematical modeling for greenhouse heating by using thermal curtain and geothermal energy. *Solar Energy,* 76**,** 603-613.

Hepbasli, A (2005). Thermodynamic analysis of a ground-source heat pump system for district heating. *International Journal of Energy Research,* 29**,** 671-687.

Hussain, MI, Ali, A and Lee, GH (2015). Performance and economic analyses of linear and spot Fresnel lens solar collectors used for greenhouse heating in South Korea. *Energy,* 90**,** 1522-1531.

Jafarkazemi, F and Ahmadifard, E (2013). Energetic and exergetic evaluation of flat plate solar collectors. *Renewable Energy,* 56**,** 55-63.

Joudi, KA and Farhan, AA (2014). Greenhouse heating by solar air heaters on the roof. *Renewable Energy,* 72**,** 406-414.

Kalogirou, SA (2013). *Solar energy engineering: processes and systems,* Academic Press.

Kalogirou, SA, Karellas, S, Badescu, V and Braimakis, K (2016a). Exergy analysis on solar thermal systems: a better understanding of their sustainability. *Renewable Energy,* 85**,** 1328-1333.

Kalogirou, SA, Karellas, S, Braimakis, K, Stanciu, C and Badescu, V (2016b). Exergy analysis of solar thermal collectors and processes. *Progress in Energy and Combustion Science,* 56**,** 106-137.

Khalifa, A and Mehdi, M (1998). On the verification of a hydrogen bubble flow meter used for monitoring flow rates in thermosyphon solar water heaters. *Energy conversion and management,* 39**,** 1295-1302.

Mehrpooya, M, Hemmatabady, H and Ahmadi, MH (2015). Optimization of performance of combined solar collector-geothermal heat pump systems to supply thermal load needed for heating greenhouses. *Energy Conversion and Management,* 97**,** 382-392.

Mortezapour, H, Ghobadian, B, Khoshtaghaza, M and Minaee, S (2012). Performance analysis of a two-way hybrid photovoltaic/thermal solar collector. *Journal of Agricultural Science and Technology,* 14**,** 767-780.

Ozgener, O and Hepbasli, A (2005). Experimental investigation of the performance of a solar-assisted ground-source heat pump system for greenhouse heating. *International Journal of Energy Research,* 29**,** 217-231.

Paksoy, M, Türkmen, Ö and Dİrek, M (2010). Importance of geothermal water using for greenhouse heating in Turkey. *Selçuk Tarım Bilimleri Dergisi,* 24**,** 50-53.

Santamouris, M, Argiriou, A and Vallindras, M (1994). Design and operation of a low energy consumption passive solar agricultural greenhouse. *Solar Energy,* 52**,** 371-378.

Shrivastava, R, Kumar, V and Untawale, S (2017). Modeling and simulation of solar water heater: A TRNSYS perspective. *Renewable and Sustainable Energy Reviews,* 67**,** 126-143.

Tiwari, G and Dhiman, N (1986). Design and optimization of a winter greenhouse for the Leh-type climate. *Energy Conversion and Management,* 26**,** 71-78.

Ureña-Sánchez, R, Callejón-Ferre, ÁJ, Pérez-Alonso, J and Carreño-Ortega, Á (2012). Greenhouse tomato production with electricity generation by roof-mounted flexible solar panels. *Scientia Agricola,* 69**,** 233-239.

Vadiee, A and Martin, V (2013). Energy analysis and thermoeconomic assessment of the closed greenhouse–The largest commercial solar building. *Applied Energy,* 102**,** 1256-1266.

Woldemichael, DE, Cheng, HK, Woldeyohannes, AD and Ing, LC (2012). Design Support System for Parabolic Trough Solar Collector. *Journal of Applied Sciences,* 12**,** 2474.

Yano, A, Onoe, M and Nakata, J (2014). Prototype semi-transparent photovoltaic modules for greenhouse roof applications. *Biosystems Engineering,* 122**,** 62-73.

Yılmaz, İH and Söylemez, MS (2014). Thermo-mathematical modeling of parabolic trough collector. *Energy Conversion and Management,* 88**,** 768-784.

Zhou, N, Yu, Y, Yi, J and Liu, R (2017). A study on thermal calculation method for a plastic greenhouse with solar energy storage and heating. *Solar Energy,* 142**,** 39-48.

.